Observation and control of Si surface and interface processes for nanostructure formation by scanning reflection electron microscopy

1999 J. Phys.: Condens. Matter 11 9861

(http://iopscience.iop.org/0953-8984/11/49/304)

J. Phys.: Condens. Matter **11** (1999) 9861–9870. Printed in the UK PII: S0953-8984(99)04271-X

Observation and control of Si surface and interface processes for nanostructure formation by scanning reflection electron microscopy

Masakazu Ichikawa

Joint Research Center for Atom Technology, 1-1-4 Higashi, Tsukuba, Ibaraki 305-0046, Japan

Received 12 May 1999

Abstract. We observe the oxidation process on clean Si surfaces using high-resolution scanning reflection electron microscopy and form nanostructures on them using focused electron-beam- (EB-) induced surface reactions. Si thermal oxidation occurs layer by layer, and the interface between the oxide film (<1 nm thickness) and Si substrate becomes atomically abrupt. When the sample is heated to 700–800 °C after being irradiated by the focused EB on the surface at room temperature, SiO_2 film is selectively decomposed from the EB-irradiated area, resulting in the exposure of a clean Si substrate. The typical width of the clean Si 'open windows' is about 10 nm. Using selective reactions during heating after the deposition of Si and Ge films on the patterned samples, Si nanowires and Ge nanoislands with 10 nm size are formed on Si surfaces. Ga-adsorbed Si nanoareas and Ga nanodots are also formed by selective adsorption of Ga on the Si window areas.

1. Introduction

Various kinds of electron microscopy have been used to observe and characterize clean surfaces, such as reflection electron microscopy (REM) [1], low-energy electron microscopy (LEEM) [2] scanning electron microscopy (SEM) [3] and scanning reflection electron microscopy (SREM) [4, 5]. Projection-type electron microscopy such as REM and LEEM is suitable for studying surface dynamic processes. Yet, scanning-type electron microscopy such as SEM and SREM is suitable for surface microanalyses and also to modify surface microareas through the use of a focused beam. This makes it possible to observe and form nanostructures on Si surfaces at the same time.

Recently, we have developed high-resolution SREMs (∼2 nm beam diameter) combined with other surface analysis techniques, such as scanning tunnelling microscopy (STM) [6], scanning Auger electron microscopy (SAM) and x-ray photoemission spectroscopy (XPS) [7]. We have applied these to the study and control of surface reaction phenomena which are useful in the formation of Si nanostructures. We have found that focused electron-beam- (EB-) induced reactions in ultra-thin SiO_2 films on Si substrates are useful for forming 10 nm size nanostructures.

It is well known that SiO_2 films decompose at random off Si surfaces through the formation of voids during heating at about 800 °C [8]. If the shape and position of the voids can be controlled, we can form clean open Si windows at given areas in SiO_2 films. We have recently found that ultra-thin SiO_2 films selectively decompose from EB-irradiated areas during heating [9, 10]. This makes it possible to form Si windows and nanostructures of 10 nm size by using selective reactions on the patterned samples to which some materials are supplied.

0953-8984/99/499861+10$30.00

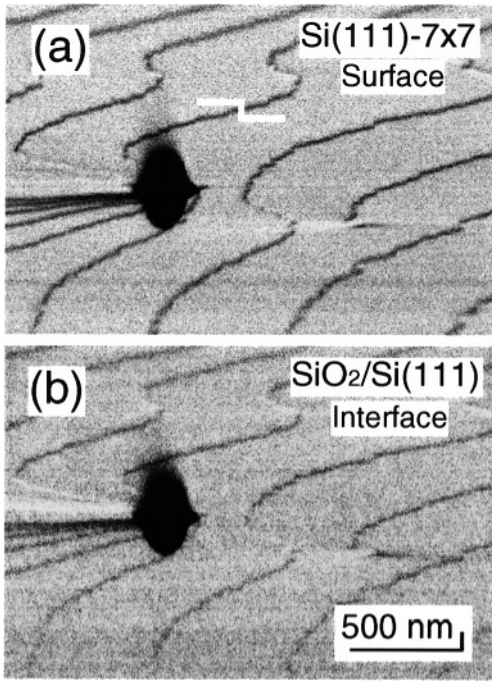

Figure 1. SREM images of (a) clean Si(111) surface and (b) the oxidized Si(111) surface. The oxide film thickness is about 0.9 nm.

2. Experiment

The experiments were performed using two kinds of SREM. In SREM, microprobe reflection high-energy electron diffraction (μ-RHEED) spot intensity is used to obtain scanning electron microscope images. Specular reflection spot intensity is mostly used for the image signal. The incident electron beam energy is 30 keV and the beam diameter is about 2 nm. The apparatus vacuum is less than 1×10^{-8} Pa. One type of SREM is combined with SEM, STM and molecular beam epitaxy (MBE) equipment [6]. Three kinds of material are simultaneously deposited on the surfaces during SREM and SEM observations. The points for STM analysis are selected by observing surfaces by SEM and SREM. The other type of SREM is combined with SEM, SAM and XPS [7]. We can obtain surface-sensitive Auger electron spectra from surface microareas and XPS spectra from surface areas (not microareas) at the same time. We partly used high temperature STM equipped with gas source MBE equipment [11].

3. Results and discussion

3.1. Observation of layer-by-layer Si oxidation

We obtained clean Si surfaces with a miscut angle of less than $1'$ by flash direct current heating at 1200 °C. The clean Si surfaces had atomic steps and atomically flat terraces. The surfaces were oxidized at 720 °C for several minutes in molecular oxygen with a partial pressure of 1.33×10^{-2} Pa. The thickness and chemical composition of the oxide films were characterized by XPS. The thickness was estimated to be less than 1 nm based on oxidation time and the oxide films were found to be mainly composed of silicon dioxide (SiO_2) [12].

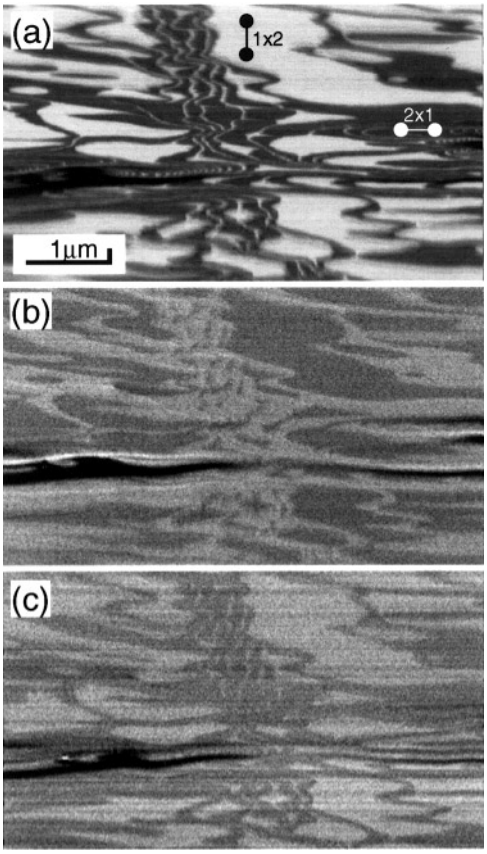

Figure 2. SREM images of (a) clean Si(001) surface, (b) after oxidation in molecular oxygen of 1.33×10^{-2} Pa at 720 °C for 30 s and (c) after additional oxidation for 60 s. The oxide film thickness of (c) is about 0.4 nm.

Figures 1(a) and (b) show SREM images of a clean Si(111) surface and an oxidized surface formed at 720 °C for 60 min, respectively. The SiO_2 film thickness was about 0.9 nm. Atomic steps, screw dislocation and atomically flat terraces can be observed on the clean surface. The same structures can be observed on the oxidized sample. This is not a surface image but an interface image between the SiO_2 film and Si(111) substrate, since amorphous SiO_2 does not contribute to the formation of an SREM image obtained using a specularly diffracted electron beam. The preservation of the structures indicates that two-dimensional (2D) nucleation oxidation takes place layer by layer during Si oxidation and the interface is atomically abrupt.

Figures 2(a), (b) and (c) show SREM images obtained using the specular reflection spot of a clean Si(001) surface, the same sample after 30 s of oxidation at 720 °C and one after an additional 60 s of oxidation, respectively. The bright and dark terrace contrasts on the clean Si surface are mainly caused by the 2×1 surface structure. The bright area has a 1×2 structure where the Si dimerization axis is parallel to the direction of the incident electron beam. The dark area has a 2×1 structure where the dimerization axis is perpendicular to the direction of the beam direction. As shown in (b) and (c), terrace contrast still remains after oxidation. This contrast is not caused by the 2×1 surface structure but the interface structure between

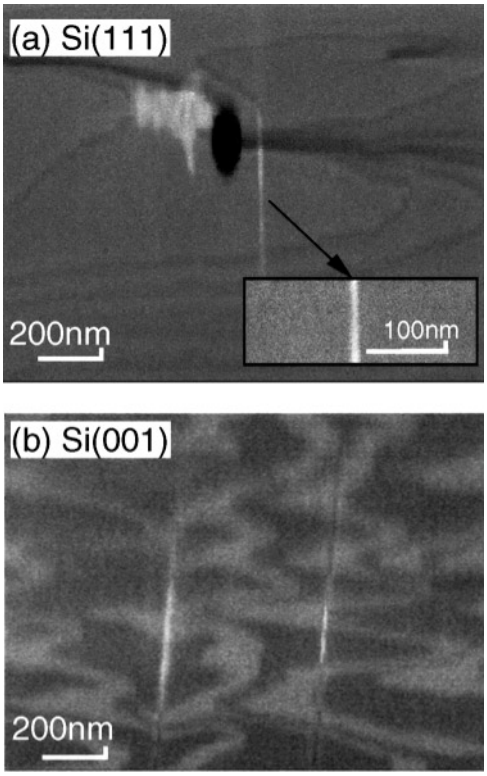

Figure 3. SREM images of SiO_2-film-covered surfaces where the film is selectively decomposed from EB-irradiated areas during heating. (a) SiO_2/Si(111), SiO_2 film thickness is 0.7 nm, (b) SiO_2/Si(001), SiO_2 thickness is 0.4 nm.

the SiO_2 and Si substrate, since the 2×1 RHEED spots disappeared and the 1×1 RHEED pattern could only be observed after oxidation. This contrast is caused by the direction of the interface Si bond between the amorphous SiO_2 film and the Si substrate. We checked, using dynamical RHEED intensity calculations, that the interface terrace brightens when the substrate Si bond at the interface is parallel to the direction of the incident beam compared with the normal direction [13]. The terrace contrast reversions in figures 2(b) and (c) are caused by the change in Si bond direction during oxidation, indicating layer-by-layer 2D nucleation oxidation. The uniformity in terrace contrast indicates an atomically abrupt interface between the SiO_2 film and Si substrate. By detecting oxygen Auger intensity at the same time, we could also measure the activation energy of oxidation at each Si layer [14].

3.2. Selective thermal decomposition of atomic-layer SiO_2 film

The focused EB used for SREM was linearly scanned on an Si(111) sample covered with the previously mentioned SiO_2 film (0.7 nm thickness) at room temperature (RT) and it was heated at 750 °C for 30 s. The EB line dose was about 5×10^{-5} C cm^{-1}. Figure 3(a) shows an SREM image of the sample. Figure 3(b) shows an Si(001) sample covered with 0.4 nm thick SiO_2 film which was manipulated in the same manner as (a). The contrast in the EB-irradiated areas did not change after EB irradiation at RT but the EB irradiated areas brightened after heating. The bright line area in figure 3(a) showed a μ-RHEED pattern from the 7×7 surface structure

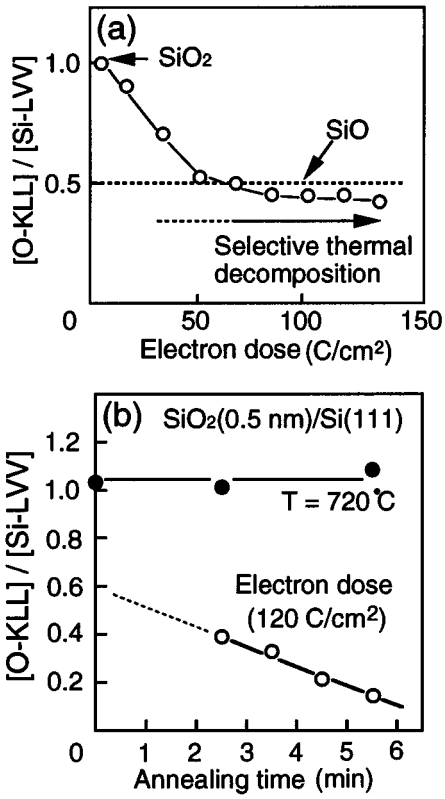

Figure 4. Intensity changes of oxygen Auger electron intensity during (a) EB irradiation and (b) annealing at 720 °C after EB irradiation at room temperature.

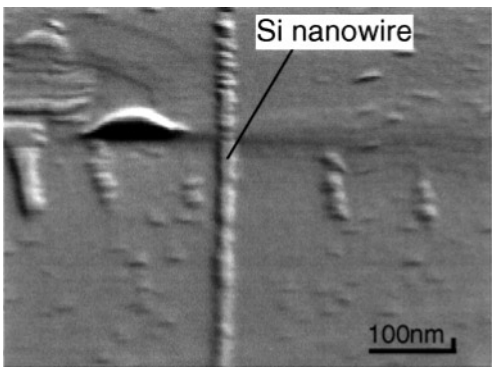

Figure 5. SEM image of Si nanowire. 4 ML Si was deposited on the surface at 530 °C and the sample was annealed at 730 °C for 30 s.

and the bright line area in figure 3(b) showed the pattern of the 2×1 surface structure. There was a 1×1 structure outside these bright line areas. This indicates that clean Si substrate surface windows appeared on the bright areas as a result of selective thermal decomposition in the SiO_2 film induced by EB irradiation. 10 nm scale clean Si windows were produced in the ultrathin SiO_2 mask. The minimum size of the window was 7 nm [10].

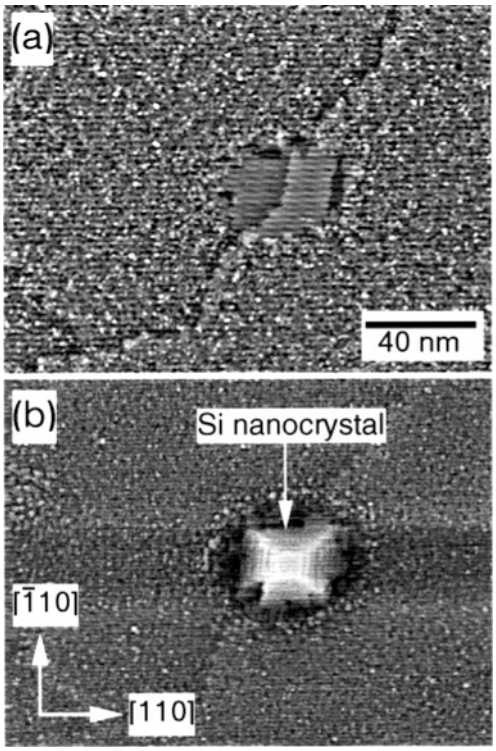

Figure 6. (a) STM image of atomic-layer SiO_2 surface with an Si window and (b) that after Si selective growth using Si_2H_6 gas at 550 °C. The SiO_2 thickness is 0.3 nm.

The mechanism for the selective thermal decomposition of SiO_2 was mainly studied by SAM [15]. It is well known that oxygen is desorbed from SiO_2 films due to the Auger process when EBs are irradiated on SiO_2 films [16]. We found that SiO_2 films changed to SiO-like films due to oxygen desorption as shown in figure 4(a). When the sample is heated, the SiO-like films easily change to volatile SiO (gas), resulting in selective thermal decomposition from the EB-irradiated area (figure 4(b)). The effect of secondary electrons is small in this process, since core level excitation energy larger than 30 eV is needed for EB-stimulated oxygen desorption [16, 17]. This indicates that the window size is mainly determined by the EB diameter.

3.3. Application to nanostructure fabrication

3.3.1. Si nanostructure on Si surface. Nanostructure fabrication was tried using the patterned sample shown in figure 3(a). Si of four-bilayer (BL) thickness was deposited on this sample at 530 °C. The epitaxial and amorphous Si films were grown on the window area and SiO_2 area, respectively. An SEM image of the sample is shown in figure 5 after it was heated at 730 °C for 30 s. Only epitaxial grown Si wires on the window area remained on the surface since the oxide film decomposed as a result of the following reaction: $Si(\text{deposited}) + SiO_2 \rightarrow 2SiO(\text{gas})$ [9]. The width of the Si wire is about 10–15 nm and the height is about 1 nm.

Si nanocrystals were also formed using selective epitaxial growth on the Si window as shown in figures 6(a) and (b) [18]. An electron-stimulated desorption study by Ueda has revealed that oxygen desorbs from a Si surface in the range of 30–300 eV and that its yield

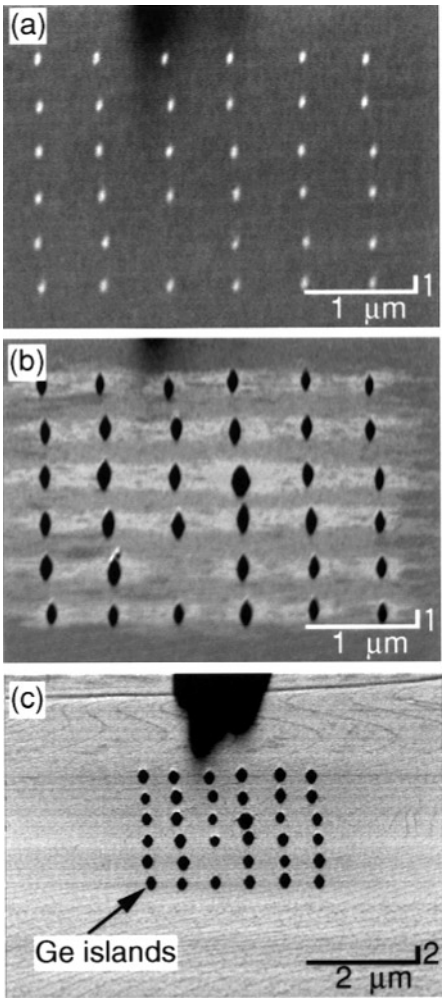

Figure 7. SREM images showing Ge island growth processes using the atomic-layer mask technology: (a) after 4 ML Ge growth at 550 °C, (b) after annealing at 690 °C for 5 min, (c) additional annealing at 690 °C for 5 min.

reaches a maximum value at 150 eV. Therefore, it is expected that a field emission (FE) electron beam from an STM tip can be used to fabricate windows in the oxide films. Figure 6(a) shows an STM image of the oxidized Si(001) surface after fabrication at 550 °C. The FE electron irradiation was done at an electron energy of 90 eV. The STM tip was 130 nm from the sample surface. A clean Si(001) surface window appeared at the FE electron-irradiated area. Figure 6(b) shows an STM image after 7 min growth at 550 °C. An Si nanocrystal with the shape of the frustum of a quadrangular pyramid is grown only in the window. This indicates that the atomic-layer SiO_2 mask can be used for nanofabrication using selective epitaxial growth.

3.3.2. Ge nanostructure on Si surface. When 4 monolayer (ML) thick Ge was deposited on the oxidized Si(111) surface with point-shaped windows at 550 °C, epitaxial and amorphous Ge films grew on the windows and SiO_2 areas, respectively as shown in figure 7(a). When the

sample was annealed at 690 °C, the SiO_2 film was reacted with the deposited Ge films, and Ge islands grew on the window areas as shown in figures 7(b), (c). It is noted that the Ge islands were grown on the window areas without any Ge islands outside the window areas [19].

During the annealing of the sample, the SiO_2 film was decomposed as a result of the following reaction: $Ge + SiO_2 \rightarrow SiO(gas) + GeO(gas)$ [10]. At the same time, excess Ge diffused to the window areas. The effective thickness became larger than 4 ML and Ge island nucleation started due to Stranski–Krastanov growth. The island size became larger by further Ge diffusion to Ge islands as shown in figure 7(c).

In the above growth condition, the Ge island size is about 200 nm. However, we can make much smaller Ge islands when the Ge thickness is decreased. Figure 8 shows an SREM image of the patterned sample after 3 ML Ge deposition at 550 °C and annealing at 690 °C for 10 min. Ge islands with 10 nm size grew only on the window areas. These results indicate a new technology for Ge quantum dot formation at given areas on Si surfaces.

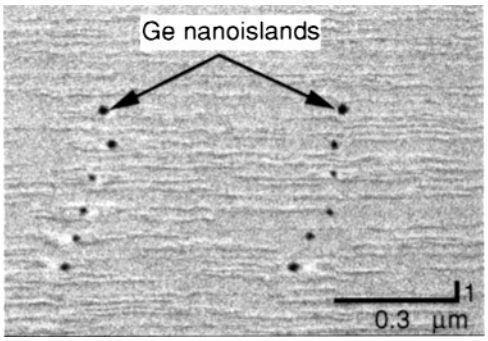

Figure 8. SREM image of Ge nanoislands formed by the atomic-layer mask technology. The growth conditions are the same as those in figure 7. The Ge film thickness was 3 ML.

3.3.3. Ga nanostructure on Si. We also tried to form Ga nanostructures using the atomic-layer SiO_2 mask technology [20]. Figure 9(a) shows an SREM image of an oxidized Si(111) surface with a Ga-adsorbed Si(111) linear window. This structure was made by 0.7 ML Ga deposition at RT and subsequent annealing at 630 °C for 2 min. The Ga desorption rate on the oxide surface is about 2.5 times larger than that on the clean Si(111) surface. Then, Ga remained only in the window area and formed a $\sqrt{3} \times \sqrt{3}$ Ga surface structure. This patterned sample is useful for doping control on the nanoscale, since Ga plays the role of p-type dopant in Si film.

Figure 9(b) shows an SREM image of an oxidized S(111) surface with point-shaped windows in which Ga dots with 20 nm size were formed. This structure was made by 0.5 ML Ga deposition at 550 °C. Deposited Ga atoms on the oxide surface migrate to the window areas to form Ga dots or desorb from the surface. This caused selective Ga dot formation in the window areas. This patterned sample is useful for GaN nanodot formation when Ga dots are nitrided.

4. Conclusion

We found that an Si open window area can be produced at given areas in ultrathin SiO_2 film using selective thermal decomposition induced by EB. When Si, Ge or Ga was supplied to such surfaces, nanostructures could be produced by selective reactions between the window area

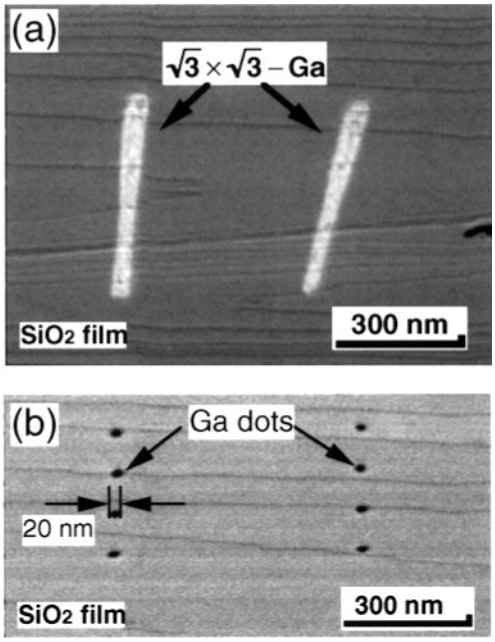

Figure 9. SREM images of Ga nanostructures formed by the atomic-layer mask technology. (a) Si(111) $\sqrt{3} \times \sqrt{3}$-Ga structure formed on the Si linear window. (b) Ga nanodots formed on the point-shaped Si windows.

and the SiO_2-covered area. The ultra-high vacuum condition used in nanostructure formation made it possible to maintain surface and interface cleanness, resulting in the fabrication of high quality nanostructures. Our approach has the possibility of being developed into a useful Si nanofabrication technique.

Acknowledgments

This study was done in collaboration with Drs S Maruno (Mitsubishi), S Fujita (Toshiba), K Fujita (Oki), Y Kusumi (Kobe Steel), H Watanabe (NEC), A Shklayev (JRCAT) M Shibata (JRCAT) and Y Nitta (JRCAT). This work was supported by the New Energy and Industrial Technology Development Organization (NEDO) and the National Institute for Advanced Interdisciplinary Research.

References

[1] Yagi K 1993 *Surf. Sci. Rep.* **17** 305
[2] Bauer E 1996 *Appl. Surf. Sci.* **92** 20
[3] Homma Y, Tomita M and Hayashi T 1991 *Surf. Sci.* **258** 147
[4] Ichikawa M 1989 *Mater. Sci. Rep.* **4** 147
[5] Liu J and Cowley J M 1993 *Ultramicroscopy* **48** 381
[6] Maruno S, Nakahara H, Fujita S, Watanabe H, Kusumi Y and Ichikawa M 1997 *Rev. Sci. Instrum.* **68** 116
[7] Watanabe H and Ichikawa M 1996 *Rev. Sci. Instrum.* **67** 4185
[8] Engel T 1993 *Surf. Sci. Rep.* **18** 91
[9] Fujita S, Maruno S, Watanabe H and Ichikawa M 1996 *Appl. Phys. Lett.* **69** 638
[10] Fujita S, Maruno S, Watanabe H and Ichikawa M 1997 *J. Vac. Sci. Technol.* A **15** 1493

[11] Fujita K, Kusumi Y and Ichikawa M 1997 *Surf. Sci.* **380** 66
[12] Watanabe H, Fujita K and Ichikawa M 1997 *Surf. Sci.* **385** L952
[13] Fujita S, Watanabe H, Maruno S, Ichikawa M and Kawamura T 1997 *Appl. Phys. Lett.* **71** 885
[14] Watanabe H, Kato K, Uda T, Fujita K, Ichikawa M, Kawamura T and Terakura K 1998 *Phys. Rev. Lett.* **80** 345
[15] Watanabe H, Fujita S, Maruno S, Fujita K and Ichikawa M 1997 *Appl. Phys. Lett.* **71** 1038
[16] Knotek M L and Feibelman P J 1978 *Phys. Rev. Lett.* **40** 964
[17] Ueda K 1994 *Japan. J. Appl. Phys.* **33** 1524
[18] Shibata M, Nitta Y, Fujita K and Ichikawa M 1998 *Appl. Phys. Lett.* **73** 2179
[19] Shklyaev A A, Shibata M and Ichikawa M 1998 *Appl. Phys. Lett.* **72** 320
[20] Shibata M, Stoyanov S and Ichikawa M 1999 *Phys. Rev.* B **59** 10 289